Langmuir
Article
pubs.acs.org/Langmuir

Oscillatory Structural Forces Due to Nonionic Surfactant Micelles: Data by Colloidal−Probe AFM vs Theory

Nikolay C. Christov,[†,‡] Krassimir D. Danov,[†] Yan Zeng,[‡] Peter A. Kralchevsky,*[,†] and Regine von Klitzing[‡]

[†]*Department of Chemical Engineering, Faculty of Chemistry, Sofia University, BG-1164 Sofia, Bulgaria, and* [‡]*Stranski-Laboratorium für Physikalische und Theoretische Chemie, Technische Universität Berlin, D-10623 Berlin, Germany*

Received July 4, 2009. Revised Manuscript Received September 13, 2009

Micellar solutions of nonionic surfactants Brij 35 and Tween 20 are confined between two surfaces in a colloidal-probe atomic-force microscope (CP-AFM). The experimentally detected oscillatory forces due to the layer-by-layer expulsion of the micelles agree very well with the theoretical predictions for hard-sphere fluids. While the experiment gives parts of the stable branches of the force curve, the theoretical model allows reconstruction of the full oscillatory curve. Therewith, the strength and range of the ordering could be determined. The resulting aggregation number from the fits of the force curves for Brij 35 is close to 70 and exhibits a slight tendency to increase with the surfactant concentration. The last layer of micelles cannot be pressed out. The measured force-vs-distance curve has nonequilibrium portions, which represent "jumps" from one to another branch of the respective equilibrium oscillatory curve. In the case of Brij 35, at concentrations < 150 mM spherical micelles are present and the oscillation period is close to the micelle diameter, slightly decreasing with the rise of concentration. For elongated micelles (at concentration 200 mM), no harmonic oscillations are observed anymore; instead, the period increases with the decrease of film thickness. In the case of Tween 20, the force oscillations are almost suppressed, which implies that the micelles of this surfactant are labile and are demolished by the hydrodynamic shear stresses due to the colloidal-probe motion. The comparison of the results for the two surfactants demonstrates that in some cases the micelles can be destroyed by the CP-AFM, but in other cases they can be stable and behave as rigid particles. This behavior correlates with the characteristic times of the slow micellar relaxation process for these surfactants.

1. Introduction

The oscillatory structural forces were first detected by means of a surface-force apparatus in organic liquids[1,2] and in aqueous solutions[3,4] confined between two smooth solid surfaces. In this context, the oscillatory forces are often called solvation or hydration forces, and their period is of the order of the molecular diameter. The force oscillation occurs when the oscillating concentration profile of the molecules, particles, or aggregates in front of the opposing surfaces overlap. With the decrease of film thickness, the layers of molecules are pressed out one after another, which leads to alternating repulsion and attraction. Under certain conditions, not the full oscillation, but only the repulsive parts are detectable, which leads to a stepwise thinning or "stratification". This was especially observed for foam films containing, e.g., surfactant micelles or latex particles.[5−11] These forces can stabilize the liquid films and disperse systems, since they hamper the film drainage.[9−14] The stable branches of the oscillatory curves have been detected by means of a thin film pressure balance.[15−19] Oscillatory forces due to surfactant micelles and microemulsion droplets have been measured by means of a surface-force apparatus,[20,21] by light-scattering method,[22] by micelle structuring in films by electron cryomicroscopy,[23,24] in asymmetric films,[25] in emulsion films,[26] and in films containing solid colloidal spheres.[5,6,27−30] Such forces are observed also in

*Corresponding author. Phone: (+359) 2-9625310. Fax: (+359) 2-9625643 E-mail: pk@lcpe.uni-sofia.bg.

(1) Horn, R. G.; Israelachvili, J. N. *J. Chem. Phys.* **1981**, *75*, 1400–1411.
(2) Christenson, H. K.; Gruen, D. W. R.; Horn, R. G.; Israelachvili, J. N. *J. Chem. Phys.* **1987**, *87*, 1834–1841.
(3) Israelachvili, J. N.; Pashley, R. M. *Nature* **1983**, *306*, 249–250.
(4) Israelachvili, J. N. *Intermolecular and Surface Forces*; Academic Press: London, 1992.
(5) Nikolov, A. D.; Wasan, D. T.; Kralchevsky, P. A.; Ivanov, I. B. In *Ordering and Organisation in Ionic Solutions*; Ise, N., Sogami, I., Eds.; World Scientific: Singapore, 1988; pp 302−314.
(6) Nikolov, A. D.; Wasan, D. T. *J. Colloid Interface Sci.* **1989**, *133*, 1–12.
(7) Nikolov, A. D.; Kralchevsky, P. A.; Ivanov, I. B.; Wasan, D. T. *J. Colloid Interface Sci.* **1989**, *133*, 13–22.
(8) Kralchevsky, P. A.; Nikolov, A. D.; Wasan, D. T.; Ivanov, I. B. *Langmuir* **1990**, *6*, 1180–1189.
(9) Nikolov, A. D.; Wasan, D. T.; Denkov, N. D.; Kralchevsky, P. A.; Ivanov, I. B. *Prog. Colloid Polym. Sci.* **1990**, *82*, 87–98.
(10) Wasan, D. T.; Nikolov, A. D.; Kralchevsky, P. A.; Ivanov, I. B. *Colloids Surf.* **1992**, *67*, 139–145.
(11) Sonin, A. A.; Langevin, D. *Europhys. Lett.* **1993**, *22*, 271–277.
(12) Basheva, E. S.; Kralchevsky, P. A.; Danov, K. D.; Ananthapadmanabhan, K. P.; Lips, A. *Phys. Chem. Chem. Phys.* **2007**, *9*, 5183–5198.
(13) Wasan, D.; Nikolov, A. *Curr. Opin. Colloid Interface Sci.* **2008**, *13*, 128–133.
(14) von Klitzing, R.; Müller, H. J. *Curr. Opin. Colloid Interface Sci.* **2002**, *7*, 42–49.
(15) Bergeron, V.; Radke, C. J. *Langmuir* **1992**, *8*, 3020–3026.
(16) Bergeron, V.; Jimenez-Laguna, A. I.; Radke, C. J. *Langmuir* **1992**, *8*, 3027–3032.
(17) Mysels, K. J.; Jones, M. N. *Discuss. Faraday Soc.* **1966**, *42*, 42–50.
(18) Exerowa, D.; Scheludko, A. *Compt. Rend. Acad. Bulg. Sci.* **1971**, *24*(47), 50.
(19) Exerowa, D.; Kolarov, T.; Khristov, K. *Colloids Surf. A* **1987**, *22*, 171–185.
(20) Richetti, P.; Kékicheff, P. *Phys. Rev. Lett.* **1992**, *68*, 1951–1954.
(21) Parker, J. L.; Richetti, P.; Kékicheff, P; Sarman, S. *Phys. Rev. Lett.* **1992**, *68*, 1955–1958.
(22) Krichevsky, O.; Stavans, J. *Phys. Rev. Lett.* **1995**, *74*, 2752–2755.
(23) Denkov, N. D.; Yoshimura, H.; Nagayama, K.; Kouyama, T. *Phys. Rev. Lett.* **1996**, *76*, 2354–2357.
(24) Denkov, N. D.; Yoshimura, H.; Nagayama, K. *Ultramicroscopy* **1996**, *65*, 147–158.
(25) Bergeron, V.; Radke, C. J. *Colloid Polym. Sci.* **1995**, *273*, 165–174.
(26) Marinova, K. G.; Gurkov, T. D.; Dimitrova, T. D.; Alargova, R. G.; Smith, D. *Langmuir* **1998**, *14*, 2011–2019.
(27) Basheva, E. S.; Nikolov, A. D.; Kralchevsky, P. A.; Ivanov, I. B.; Wasan, D. T. In *Surfactants in Solution*; Mittal, K. L., Ed.; Plenum Press: New York, 1991; Vol. *11*, pp 467−479.
(28) Basheva, E. S.; Danov, K. D.; Kralchevsky, P. A. *Langmuir* **1997**, *13*, 4342–4348.
(29) Sethumadhavan, G. N.; Nikolov, A. D.; Wasan, D. T. *J. Colloid Interface Sci.* **2001**, *240*, 105–112.
(30) Klapp, S. H. L.; Zeng, Y.; Qu, D.; von Klitzing, R. *Phys. Rev. Lett.* **2008**, *100*, 118303.

more complex systems like protein solutions, surfactant−polymer mixtures, solutions of polyelectrolytes, and amphiphilic block copolymers.[31−42]

The developed theories are based on modeling by means of the integral equations of statistical mechanics[43−46] and numerical simulations.[30,47−52] As a rule, these approaches are related to complicated theoretical expressions or numerical procedures. To overcome this difficulty, some relatively simple semiempirical expressions have been proposed[53,54] on the basis of fits of theoretical results for hard-sphere fluids. In a recent study,[12] such a model was applied to determine the micelle size, volume fraction, and aggregation number from the experimental stepwise transitions in the thickness of free liquid films and their contact angles.

After its introduction in 1991, colloidal-probe atomic-force microscopy (CP-AFM)[55,56] has found numerous applications for measurements of surface and adhesive forces,[30,41,57−68] for the interactions of deformable particles,[69] and for living cells.[70] Recent reviews can be found in refs 71 and 72. In the case of oscillatory forces, the CP-AFM was successfully applied to study solvation forces in organic liquids[68] and in suspensions of solid nanoparticles,[30,59−62] polymers, and polyelectrolytes.[41,62−64,73] Despite the fact that some of the first manifestations of oscillatory forces have been detected with micellar surfactant solutions,[5−7] there are only three applications of CP-AFM to micellar systems.[65−67] Well-pronounced oscillations in the measured force have been detected in two of them,[66,67] for micellar solutions of sodium dodecyl sulfate (SDS). In the case of ionic surfactants, such as SDS, the oscillatory forces are essentially affected by the electric double layers around the micelles.[6,7,50,59] Unfortunately, in this case a quantitative theoretical model, which is applicable for experimental data processing, is still missing.

In the case of nonionic micelles that can be modeled as hard spheres, Trokhymchuk et al.[54] proposed a quantitative analytical expression for the oscillatory force, which has been tested against both Monte Carlo simulation data[54] and data for stratifying free foam films.[12] The aim of the present paper is to clarify the strength and the range of the ordering of the micelles under geometrical confinement. To get information about the complete oscillatory force curve, a colloidal probe AFM was used in experiments with micellar solutions of the nonionic surfactants Brij 35 and Tween 20. The data were analyzed by means of the hard-sphere theoretical model.[54]

2. Materials and Experimental Procedures

The nonionic surfactants, polyoxyethylene (23) lauryl ether (Brij 35), and polyoxyethylene (20) sorbitan monolaurate (Tween 20), products of Sigma, were used without further purification. The molecular weight of Brij 35 is 1198 g/mol; its critical micellization concentration (CMC) is 9×10^{-5} M,[74,75] and the micelle diameter is $d = 8.8$ nm.[12,76] The micelles are spherical up to 150 mM Brij 35 concentration, but they undergo a transition to elongated micelles at higher concentrations; see section 4.2 for details. The molecular mass of Tween 20 is 1225 g/mol; its CMC is 60 mg/L or 4.9×10^{-5} M,[77] and the micelle diameter is $d = 7.2$ nm.[12] In the AFM experiments, the substrates were polished silicon wafers from Wacker Siltronic (Burghausen, Germany) with native silica top layer. The particles used as colloidal probes for AFM were monodisperse silica spheres of radius 3.33 μm produced by Bangs Laboratories Inc. The particles were glued to tipless silicon cantilevers (CSC12) produced by MicroMasch (Estonia). The glue was two component epoxy (UHU plus endfest 300). All glassware was cleaned with hot Piranha solution (3 parts concentrated H_2SO_4 and 1 part H_2O_2). ***Caution***: Piranha solution reacts violently with organic matter and should be handled with extreme care!

The water was purified with Milli-Q system (Millipore Inc.) that was equipped with 220 nm filter. Ethanol (> 99.5%, extra pure), hydrogen peroxide (30%, for synthesis), and concentrated sulfuric acid (95−98%, p.a.) were supplied by Carl Roth GmbH (Karlsruhe, Germany) and were used as received.

The silicon wafers were cut in pieces and put in hot piranha solution for at least 1 h. After that, they were abundantly rinsed

(31) Koczo, K.; Nikolov, A. D.; Wasan, D. T.; Borwankar, R. P.; Gonsalves, A. *J. Colloid Interface Sci.* **1996**, *178*, 694–702.
(32) Asnacios, A.; Espert, A.; Colin, A.; Langevin, D. *Phys. Rev. Lett.* **1997**, *78*, 4974–4977.
(33) Bergeron, V.; Claesson, P. M. *Adv. Colloid Interface Sci.* **2002**, *96*, 1–20.
(34) Kolaric, B.; Förster, S.; von Klitzing, R. *Prog. Colloid Polym. Sci.* **2001**, *117*, 195–199.
(35) Kolaric, B.; Jaeger, W.; von Klitzing, R. *J. Phys. Chem. B* **2000**, *104*, 5096–5101.
(36) von Klitzing, R.; Kolaric, B.; Jaeger, W.; Brandt, A. *Phys. Chem. Chem. Phys.* **2002**, *4*, 1907–1914.
(37) Stubenrauch, C.; von Klitzing, R. *J. Phys.: Condens. Matter* **2003**, *15*, R1197–R1232.
(38) Beltran, C. M.; Guillot, S.; Langevin, D. *Macromolecules* **2003**, *36*, 8506–8512.
(39) Beltran, C. M.; Langevin, D. *Phys. Rev. Lett.* **2005**, *94*, 217803.
(40) Heinig, P.; Beltran, C. M.; Langevin, D. *Phys. Rev. E* **2006**, *73*, 051607.
(41) Qu, D.; Brotons, G.; Bosio, V.; Fery, A.; Salditt, T.; Langevin, D.; von Klitzing, R. *Colloids Surf. A* **2007**, *303*, 97–109.
(42) Kleinschmidt, F.; Stubenrauch, C.; Delacotte, J.; von Klitzing, R.; Langevin, D. *J. Phys. Chem. B* **2009**, *113*, 3972–3980.
(43) Henderson, D. *J. Colloid Interface Sci.* **1988**, *121*, 486–490.
(44) Kjellander, R.; Sarman, S. *Chem. Phys. Lett.* **1988**, *149*, 102–108.
(45) Attard, P.; Parker, J. L. *J. Phys. Chem.* **1992**, *96*, 5086–5093.
(46) Pollard, M. L.; Radke, C. J. *J. Chem. Phys.* **1994**, *101*, 6979–6991.
(47) Chu, X. L.; Nikolov, A. D.; Wasan, D. T. *Langmuir* **1994**, *10*, 4403–4408.
(48) Chu, X. L.; Nikolov, A. D.; Wasan, D. T. *J. Chem. Phys.* **1995**, *103*, 6653–6661.
(49) Trokhymchuk, A.; Henderson, D.; Nikolov, A. D.; Wasan, D. T. *J. Phys. Chem. B* **2003**, *107*, 3927–3937.
(50) Trokhymchuk, A.; Henderson, D.; Nikolov, A.; Wasan, D. T. *Langmuir* **2005**, *21*, 10240–10250.
(51) Blawzdziewicz, J.; Wajnryb, E. *Europhys. Lett.* **2005**, *71*, 269–275.
(52) Blawzdziewicz, J.; Wajnryb, E. *J. Chem. Phys.* **2008**, *129*, 194509.
(53) Kralchevsky, P. A.; Denkov, N. D. *Chem. Phys. Lett.* **1995**, *240*, 385–392.
(54) Trokhymchuk, A.; Henderson, D.; Nikolov, A.; Wasan, D. T. *Langmuir* **2001**, *17*, 4940–4947.
(55) Ducker, W. A.; Senden, T. J.; Pashley, R. M. *Nature* **1991**, *353*, 239–241.
(56) Butt, H.-J. *Biophys. J.* **1991**, *60*, 1438–1444.
(57) Butt, H.-J.; Kappl, M.; Mueller, H.; Raiteri, R.; Meyer, W.; Rühe, J. *Langmuir* **1999**, *15*, 2559–2565.
(58) Vakarelski, I. U.; Ishimura, K.; Higashitani, K. *J. Colloid Interface Sci.* **2000**, *227*, 111–118.
(59) Klapp, S. H. L.; Grandner, S.; Zeng, Y.; von Klitzing, R. *J. Phys.-Condensed Matter* **2008**, *20*, 494232.
(60) Drelich, J.; Long, J.; Xu, Z.; Masliyah, J.; Nalaskowski, J.; Beauchamp, R.; Liu, Y. *J. Colloid Interface Sci.* **2006**, *301*, 511–522.
(61) Piech, M.; Walz, J. Y. *J. Colloid Interface Sci.* **2002**, *253*, 117–129.
(62) Piech, M.; Walz, J. Y. *J. Phys. Chem. B* **2004**, *108*, 9177–9188.
(63) Milling, A. J.; Kendall, K. *Langmuir* **2000**, *16*, 5108–5115.
(64) Biggs, S.; Prieve, D.; Dagastine, R. *Langmuir* **2005**, *21*, 5421–5428.
(65) McNamee, C. E.; Tsujii, Y.; Matsumoto, M. *Langmuir* **2004**, *20*, 1791–1798.
(66) McNamee, C. E.; Tsujii, Y.; Ohshima, H.; Matsumoto, M. *Langmuir* **2004**, *20*, 1953–1962.
(67) Tulpar, A.; Van Tassel, P. R.; Walz, J. Y. *Langmuir* **2006**, *22*, 2876–2883.
(68) Lim, L. T. W.; Wee, A. T. S.; O'Shea, S. J. *Langmuir* **2008**, *24*, 2271–2273.
(69) Vakarelski, I. U.; Lee, J.; Dagastine, R. R.; Chan, D. Y. C.; Stevens, G. W.; Grieser, F. *Langmuir* **2008**, *24*, 603–605.
(70) McNamee, C. E.; Pyo, N.; Tanaka, S.; Vakarelski, I. U.; Kanda, Y.; Higashitani, K. *Colloids Surf. B* **2006**, *48*, 176–182.
(71) Butt, H.-J.; Capella, B.; Kappl, M. *Surf. Sci. Rep.* **2005**, *59*, 1–152.
(72) Bonaccurso, E.; Kappl, M.; Butt, H.-J. *Curr. Opin. Colloid Interface Sci.* **2008**, *13*, 107–119.
(73) Qu, D.; Pedersen, J. S.; Garnier, S.; Laschewsky, A.; Möhwald, H.; von Klitzing, R. *Macromolecules* **2006**, *39*, 7364–7371.
(74) Schick, M. J. *Nonionic Surfactants: Surfactant Science Series*; Marcel Dekker: New York, 1987; Vol. *23*.
(75) Sharma, K. S.; Patil, S. R.; Rakshit, A. K.; Glenn, K.; Doiron, M.; Palepu, R. M.; Hassan, P. A. *J. Phys. Chem. B* **2004**, *108*, 12804–12812.
(76) J. Phillies, G. D.; Hunt, R. H.; Strang, K.; Sushkin, N. *Langmuir* **1995**, *11*, 3408–3416.
(77) Helenius, A.; McCaslin, D. R.; Fries, E.; Tanford, C. *Method. Enzymol.* **1979**, *56*, 734–749.

with pure water and stored in ethanol. Just before the experiment, the substrate was taken out of the ethanol and dried in a nitrogen flux.

The silica particles were glued at the end of a 350 μm rectangular tipless cantilever with nominal spring constant of 0.03 N/m. The manipulations were carried out by a micromanipulator on an inverted microscope equipped with a 40× long-distance objective lens.

The measurements of the interaction force between the silicon substrate and the silica particle across a micellar surfactant solution were carried out with a MFP-1D atomic force microscope (Asylum Research Inc.). The scanning frequencies were varied from 0.05 to 0.4 Hz over a force distance of 100−1250 nm. The corresponding velocities of approach−retraction of probe were between 5 and 500 nm/s. All experiments were carried out at room temperature 23 ± 2 °C.

At the beginning of each experiment, the tip holder was cleaned carefully with ethanol and water. The silicon substrate was attached to a clean microscope slide, and 7−10 drops of the studied solution were placed on the silicon surface. The tip with the attached particle was manually approached in the solution until nearly in contact with the substrate and was held there at least 15 min before force measuring. The spring constant of each cantilever was determined by the thermal noise method and was typically in the range 0.01−0.05 N/m. The force−distance profile was estimated from the raw deflection vs displacement curves. At every concentration, the experiment was repeated two or three times, with different cantilevers and substrates. Multiple runs, at different lateral positions, were performed in each experiment.

3. Theoretical Section

Using the Derjaguin's approximation,[4,78,79] one can express the surface force, F, between a spherical particle and a planar plate in the form:

$$F(H) = 2\pi R W(H) = 2\pi R \int_H^\infty \Pi(\check{H})\, \mathrm{d}\check{H} \tag{1}$$

where R is the particle radius, H is the surface-to-surface distance between the particle and the plate, $W(H)$ is the interaction energy per unit area of a plane-parallel liquid film of thickness H, Π is the disjoining pressure, and $\check{H}$ is an integration variable. In the considered case of nonionic surfactant micelles, W can be expressed as a sum of contributions from the van der Waals forces, W_{vw}, and oscillatory structural forces due to the surfactant micelles, W_{osc}:[4,12]

$$W(H) = W_{osc} + W_{vw} = W_{osc} - \frac{A_H}{12\pi H^2} \tag{2}$$

where A_H is the Hamaker constant. The surface charge of the outer confining silica surfaces can be neglected, since nonionic surfactant is partially adsorbed at the surface (see below). Introducing surface charge would not change the oscillation period and decay length but would increase the amplitude w_0;[41] see eq 5 for the notations. When comparing the hard-sphere theory with the experiment without using adjustable parameters, we did not notice deviations that could be interpreted as an effect of surface charges.

The combination of eqs 1 and 2 yields

$$F = 2\pi R \frac{kT}{d^2}\left(\frac{W_{osc} d^2}{kT} - \frac{A_H}{12\pi h^2 kT}\right) \tag{3}$$

where $h \equiv H/d$ is the dimensionless surface-to-surface distance, d is the micelle diameter, k is the Boltzmann constant, and T is the absolute temperature. Furthermore, the expression for W_{osc} due to Trokhymchuk et al.:[54] was used

$$\frac{W_{osc} d^2}{kT} = -\frac{p_{hs} d^3}{kT}(1-h) - \frac{2\sigma_{hs} d^2}{kT}, \text{ for } 0 \le h < 1 \tag{4}$$

$$\frac{W_{osc} d^2}{kT} = w_0 \cos(\omega h + \varphi_1) \mathrm{e}^{-qh} + w_1 \mathrm{e}^{\delta(1-h)}, \text{ for } h \ge 1 \tag{5}$$

where p_{hs} is the pressure of a hard-sphere fluid expressed through the Carnahan−Starling formula,[80] and σ_{hs} is the scaled-particle-theory[81] expression for the excess surface free energy of a hard-sphere fluid:

$$\frac{p_{hs} d^3}{kT} = \frac{6}{\pi}\phi \frac{1 + \phi + \phi^2 - \phi^3}{(1-\phi)^3} \tag{6}$$

$$\frac{\sigma_{hs} d^2}{kT} = -\frac{9}{2\pi}\phi^2 \frac{1+\phi}{(1-\phi)^3} \tag{7}$$

The parameters w_0, ω, φ_1, q, w_1, and δ in eq 5 depend on the hard-sphere (micelle) volume fraction, ϕ, as follows:[54]

$$w_0 = 0.57909 + 0.83439\phi + 8.65315\phi^2 \tag{8}$$

$$\omega = 4.45160 + 7.10586\phi - 8.30671\phi^2 + 8.29751\phi^3 \tag{9}$$

$$q = 4.78366 - 19.64378\phi + 37.37944\phi^2 - 30.59647\phi^3 \tag{10}$$

$$w_1 = -\frac{2\sigma_{hs} d^2}{kT} - w_0 \cos(\omega + \varphi_1) \exp(-q) \tag{11}$$

$$\varphi_1 = 0.40095 + 2.10336\phi \text{ and } \delta = \frac{\pi_1}{w_1} \tag{12}$$

where

$$\pi_1 = \frac{6}{\pi}\phi \exp\left(\frac{\Delta\mu_{hs}}{kT}\right) - \frac{p_{hs} d^3}{kT} - \pi_0 \cos(\omega + \varphi_2) \exp(-q) \tag{13}$$

$$\frac{\mu_{hs}}{kT} = \phi \frac{8 - 9\phi + 3\phi^2}{(1-\phi)^3} \tag{14}$$

$$\pi_0 = 4.06281 - 3.10572\phi + 76.67381\phi^2 \tag{15}$$

$$\varphi_2 = -0.39687 - 0.3948\phi + 2.3027\phi^2 \tag{16}$$

The parameters w_0, ω, and q defined by eqs 8−10 characterize, respectively, the amplitude, period, and decay length of the oscillations; see eq 5. The last term in eq 5 ensures the correct height of the first (the highest) maximum.[54] Note that for a hard-sphere fluid, the amplitude, period, and decay length of the oscillations depend on the particle volume fraction, ϕ, in accordance with eqs 8−10.

Equations 4−16 were applied for determination of the diameter, d, and aggregation number, N_{agg}, of Brij 35 and Tween 20 micelles from data for the thickness and contact angles of foam films and good agreement with independent data for d and N_{agg}

(78) Derjaguin, B. V. *Kolloid Z.* **1934**, *69*, 155–164.
(79) Derjaguin, B. V.; Churaev, N. V.; Muller, V. M. *Surface Forces*; Plenum Press: New York, 1987.
(80) Carnahan, N. F.; Starling, K. E. *J. Chem. Phys.* **1969**, *51*, 635–636.
(81) Reiss, H.; Frisch, H. L.; Helfand, E.; Lebowitz, J. L. *J. Chem. Phys.* **1960**, *32*, 119–124.

was obtained.[12] The relation between d, ϕ, and N_{agg}, is[12]

$$N_{agg} = \frac{\pi d^3}{6\phi}(C_s - \mathrm{CMC}) \qquad \text{for spherical micelles} \qquad (17)$$

where C_s is the total surfactant concentration and, as usual, CMC is the critical micellization concentration.

Equation 3, along with eqs 4−16, determines the theoretical dependence $F(H,\phi)$ at given colloidal probe radius, R, and micelle diameter, d. In particular, for a given micelle volume fraction, ϕ, we first calculate p_{hs}, σ_{hs}, w_0, ω, q, μ_{hs}, π_0, and φ_2 from eqs 6−10 and 14−16; after that, we calculate w_1, φ_1, π_1, and δ from eqs 11−13; next, W_{osc} is computed from eqs 4−5, and finally F, from eq 3.

The fitting procedure is as follows. The experimental force, F_{exp} is given as a function of the experimental distance, $H_{exp} = H + \Delta H$, where H is the theoretical distance and ΔH is the difference between the positions of the experimental and theoretical coordinate origins on the H-axis. The fitting by means of the least-squares method consists in numerical minimization of the following merit function:

$$\Phi(\Delta H,\phi) = \sum_i \left[F(H_{exp}^{(i)} - \Delta H,\phi) - F_{exp}^{(i)}(H_{exp}^{(i)})\right]^2 \qquad (18)$$

where $F_{exp}^{(i)}(H_{exp}^{(i)})$ is the set of experimental data numbered by the index i, and the summation is carried out over all experimental points. It is important to note that in the fitting procedure, the points from the nonequilibrium portions of the experimental curves (denoted by tangential arrows in Figures 1−4 and 6) have to be excluded, because the theoretical curve gives the equilibrium force-vs-distance dependence.

When ϕ is known from ref 12, the variation of ΔH is equivalent to a simple horizontal translation of the experimental curve with respect to the theoretical one, the latter being uniquely determined. The minimization of Φ with respect to ΔH corresponds to the best coincidence of the two curves. When ϕ is not known, we varied both ΔH and ϕ to minimize numerically Φ in eq 18, and to find the best fit. After that, substituting the obtained ϕ in eq 17, we determine the micelle aggregation number, N_{agg}.

When the theoretical curves (the solid lines in Figures 1−6) are calculated, in eq 3 the value $A_H = 7 \times 10^{-21}$ J of the Hamaker constant for silica/water/silica films was used.[4] The effect of van der Waals forces is essential only at the lowest investigated micellar concentrations, where the oscillatory amplitude w_0 is relatively small.

4. Results and Discussion

4.1. Results for Brij 35: Spherical Micelles. Figure 1 shows experimental data for 80 mM Brij 35 solution. The speed of approach and retraction was 100 nm/s. The micellar volume fraction $\phi = 0.257$ was taken from ref 12. Then, all parameters in the theoretical $F(H)$ dependence given by eqs 3−16, are known and the $F(H)$ curve in Figure 1 has been drawn without using any adjustable parameters. The experimental approach and retraction curves for F vs H were translated parallel to the horizontal axis until they overlapped with the theoretical curve in the region of greater distances. Such translation is admissible because the experimental zero on the H-axis is determined with a relatively low accuracy. In colloidal probe AFM measurements, the point of contact ($H = 0$) is usually determined by a sudden increase in deflection of the cantilever during the approach. The error is on the order of nanometers and is due to the low force constant of the used cantilevers. A coupling to an (optical) interferometric method would overcome this problem but was not used in the present study.

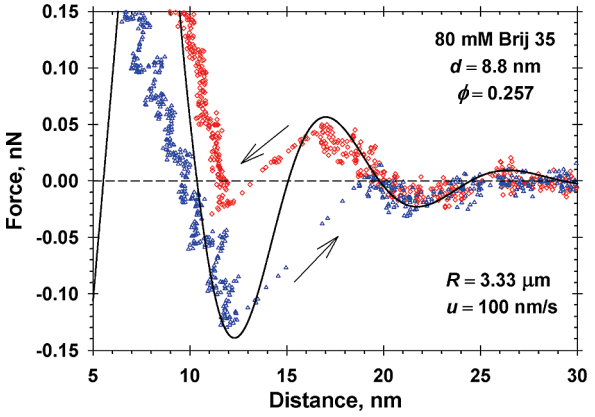

Figure 1. Force F vs distance H for a 80 mM Brij 35 aqueous solution. The points are CP-AFM data; the arrows show the direction of measuring motion: approach and retraction. The solid line is the theoretical curve drawn by means of eqs 3−16 without using adjustable parameters. The micelle mean diameter, d, volume fraction, ϕ, the probe radius, R, and velocity, u, are given in the figure.

To determine the zero on the axis of distances, we proceeded in the following way. The theoretical curves, like those in Figures 1 and 2, are independently calculated (no adjustable parameters) at known micelle diameter, d, and volume fraction, ϕ. Next, the experimental data are translated left or right, until the best coincidence with the theoretical curve is achieved. Then the zero of the *theoretical* curve is accepted as the coordinate origin, $H = 0$, for the experimental data.

If the silica surfaces are covered by surfactant adsorption layers (or dense layers of adsorbed micelles), as observed in the experiments by Ducker et al.,[82] the above definition of coordinate origin implies that the surface-to-surface distance, H, corresponds to the separation between the outer ends of the surfactant adsorption layers, rather than between the underlying silica surfaces. Upon further pressing the two surfaces against each other, it is possible to deform the surfactant layers adsorbed on the silica. The resulting short-range interaction has been already investigated,[82] and it is not a subject of the present paper, which is focused on the oscillatory force.

At both approach and retraction, jumps (denoted by arrows in the figures) from one mechanically stable branch of the oscillatory curve to the next one were observed. Such jumps have been observed also in other experimental studies, including foam film studies, where oscillatory forces were detected.[12,15,35,36,42,66,67] For the approach curves, the barriers are the oscillatory maxima, whose right branches correspond to mechanically stable states. In contrast, for the retraction curves the barriers are the oscillatory minima, whose left branches correspond to stable states. For the data in Figure 1, the jumps happen close to the tops of the respective barriers. The theoretical and experimental curves are in good agreement exceptionally at short distances. At the shorter distances ($H < 12$ nm), one micellar layer is trapped between the two solid surfaces and its deformability can be a possible explanation for (i) the difference between the experimental approach and retraction curves (hysteresis) and (ii) some deviations of each of them from the theoretical curve at the smaller H.

The plot of force on the ordinate axis in Figure 1 visualizes the typical range (0.1 nN) and the accuracy (limited by perturbations) in these experiments. In all subsequent figures, we have plotted the

(82) Grant, L. M.; Tiberg, F.; Ducker, W. A. *J. Phys. Chem. B* **1998**, *102*, 4288–4294.

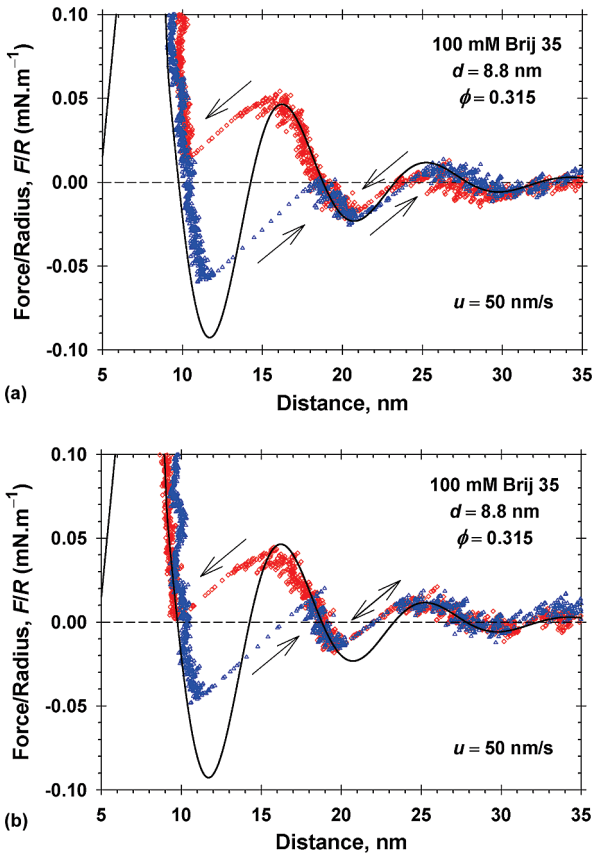

Figure 2. Illustration of the reproducibility of the experimental curves for two different runs with 100 mM Brij 35 solutions (the same cantilever, the same substrate but at two different lateral positions). The points are CP-AFM data for force F vs distance H; the arrows show the direction of motion; u = 50 nm/s is the approach/retraction velocity. The solid lines are the theoretical curves drawn by means of eqs 3−16 without using adjustable parameters.

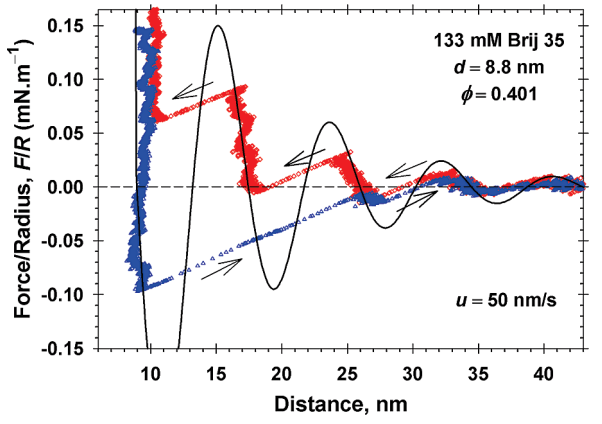

Figure 3. Force F vs distance H for a 133 mM Brij 35 solution. The points are CP−AFM data; the arrows show the direction of motion; u = 50 nm/s is the approach/retraction velocity. The solid line is the theoretical fit drawn by eqs 3−16 using the micelle volume fraction ϕ as a single adjustable parameter.

ratio force/radius, following the tradition in the surface-force measurements. In all experiments, the colloidal probe radius was the same, $R = 3.3$ μm.

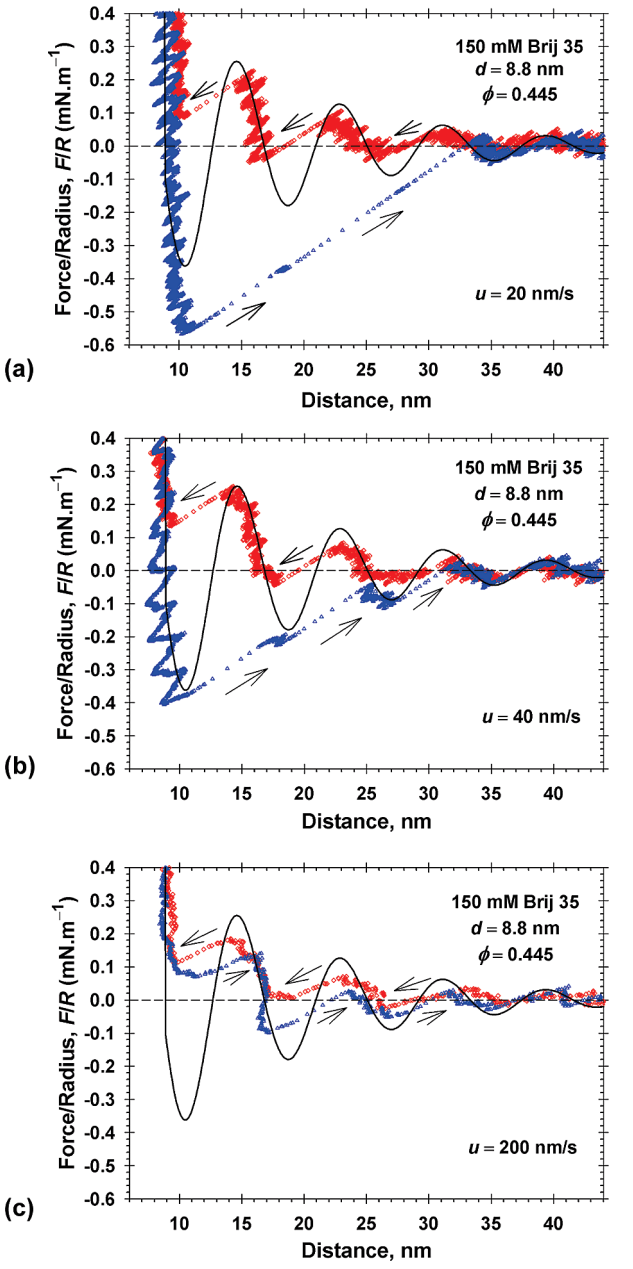

Figure 4. Effect of the rate of measuring motion: force F vs distance H for 150 mM Brij 35 solutions. The points are CP−AFM data; the arrows show the direction of motion. The solid lines are fits drawn by eqs 3−16 using the micelle volume fraction ϕ as a single adjustable parameter. The velocity of the colloidal probe is (a) u = 20 nm/s; (b) u = 40 nm/s; (c) u = 200 nm/s.

To compare the measured oscillatory force with the hydrodynamic interactions, we will use the Taylor formula[83,84] for the force of hydrodynamic interaction between a spherical particle of radius R moving with velocity u toward a planar solid surface:

$$F_{\mathrm{Ta}} = \frac{6\pi\eta u}{H} R^2 \qquad (19)$$

see, e.g., the derivation of eq 2.8.13 in ref 85. As usual, h is the shortest surface-to-surface distance from the particle to the planar solid surface, and η is the viscosity of the liquid phase.

(83) Taylor, G. I. Private communication acknowledged by: Hardy, W.; Bircumshaw, I. *Proc. R. Soc. London A* **1925**, *108*, 1−27.

(84) Horn, R. G.; Vinogradova, O. I.; Mackay, M. E.; Phan-Thien, N. *J. Chem. Phys.* **2000**, *112*, 6424–6433.

(85) Russel, W. B.; Saville, D. A; Schowalter, W. R. *Colloidal Dispersions*; Cambridge University Press: Cambridge, U.K., 1989.

The substitution of $\eta = 10^{-3}$ Pa s, $R = 3.3 \times 10^{-6}$ m, $H = 10$ nm, and $u = 100$ nm/s in eq 19 yields $F_{Ta} = 2.05 \times 10^{-3}$ nN. The latter value is equal to one-fifth of the smallest scale division on the ordinate axis in Figure 1. Hence, under the conditions of our experiments, the hydrodynamic force is negligible in comparison with the magnitude of the oscillatory force.

In Figure 2, the Brij 35 concentration is higher, 100 mM, and the amplitude of the oscillations is larger. The micellar volume fraction, $\phi = 0.315$, was taken from ref 12, so that the theoretical curve is independently determined again without adjusting any parameters. Parts a and b of Figure 2 illustrate the reproducibility of the experimental data, which is good except for some differences in the regions of the jumps that have stochastic character. It is interesting to note that in these figures the jumps upon approach happen near the top of the barrier, whereas the jumps upon retraction occur well before the top of the barrier.

In Figure 3, the Brij 35 concentration is 133 mM. For this concentration, literature data for ϕ are missing. Therefore, the micellar volume fraction was determined from the data fit, which yielded $\phi = 0.401$. The comparison between experimental and theoretical data implies that jumps occur well below the theoretical maxima and above the minima, respectively. The branches have a steeper slope than at lower concentrations (Figures 1 and 2), which indicates that the micelle layers are less compressible. At a distance of about 9−10 nm, a strong repulsion was measured, but no further material could be pressed out. Upon retraction, the particle jumps from this first minimum, over the second one, up to the third minimum's stable branch. This behavior can be explained by the fact that a strong attraction between the surfaces leads to a sudden jump out of contact; the energy, accumulated during the climbing of the energy barrier, is suddenly released and the system jumps back to a large distance.

Figure 4 illustrates the effect of the experimental velocity, u, on the measured force-vs-distance dependence for 150 mM Brij 35. At this concentration, literature data for ϕ are missing, so the micelle volume fraction was determined as an adjustable parameter from the data fit with $\phi = 0.445$. The latter value is below the Alder phase transition for hard spheres at $\phi = 0.494$.[86,87]

In Figure 4a,b, the experimental velocities are in the range of optimum velocities for approach and retraction of the colloidal probe against the planar silica surface. Below this range of speeds, the hydrodynamic drift and the noise (that modulates the obtained curves) is too high. Above the optimum speed, the system cannot rearrange fast enough after the expulsion of one layer of micelles. The latter case is illustrated in Figure 4c, where it is seen that at a greater speed ($u = 200$ nm/s) the registered oscillatory amplitude is smaller, which indicates a lower degree of structuring of the micelles within the film. In Figure 4a, the first transition upon retraction happens below the theoretical minimum, which indicates adhesion in this special case.

As mentioned above, the comparison of Figure 4c with Figure 4a,b shows that the transitions from one stable-equilibrium branch of the oscillatory curve to the next one happens easier (at smaller magnitude of the applied force) when the velocity u of the colloidal probe is greater. We recall that the oscillatory maxima represent barriers against film thinning upon approach of the colloidal probe, whereas the oscillatory minima represent barriers against film thickening upon retraction. In other words, the system opposes the applied external force tending to minimize the changes produced by it, in agreement with the Le Chatelier's principle. In the *ideal* case of quasi-static probe motion (infinitesimally small u and perfect particle structuring), the transitions should happen at the tops of the respective barriers. However, in the *real* experiment the colloidal probe moves with a finite velocity u, and the resulting hydrodynamic flow perturbs the particle (micelle) structuring. The perturbed structure yields easier, and the transition from one stable branch to the next one occurs at a smaller value of the applied external force, i.e., below the top of the respective quasi-static barrier. This effect is greater at higher speeds of particle motion in agreement with the experimental observations (Figure 4).

Comparing Figures 2, 3, and 4b that show results at more or less the same speed but different surfactant concentrations reveals an increase in the slope of the force branches. This is related to larger amplitude, w_0, of the force oscillation at greater micelle volume fraction ϕ (see Table 1). As known from previous theoretical studies,[53] the period of oscillations, characterized by the dimensionless wavelength $\lambda = 2\pi/\omega$, decreases, whereas the decay length, q^{-1}, increases with the rise of ϕ. To illustrate these effects for the investigated system, in Table 1 we have listed the values of w_0, λ, and q^{-1} calculated from eqs 8−10 for the respective ϕ values. One sees that λ is close to 1 but still varies in the framework of 16%. In contrast, the variation of the decay length is much stronger: q^{-1} increases with a factor of ca. 3 (Table 1). In other words, the micelle structuring penetrates at a thrice longer distance from the film surface.

With increasing concentration, the first minimum at a short distances during retraction becomes deeper, which indicates a stronger adhesive depletion force. As a consequence, the systems jumps back to larger distances, as already discussed in relation to Figure 3. This effect becomes stronger at lower speed (compare Figure 4a,c). At a speed of 20 nm/s, the system jumps from the first minimum, over the second and third ones, up to the fourth minimum (Figure 4a).

From the values of the micelle volume fraction, ϕ, determined from the data fits, the aggregation number, N_{agg}, of the Brij 35 micelles was determined using eq 17. The results are summarized in Table 1.

As seen in the table, N_{agg} exhibits a slight tendency to increase with the surfactant concentration, which is in agreement with the results in ref 12. At 80 and 100 mM Brij 35, the values of N_{agg} were obtained in ref 12 by interferometric contact angle measurements, and then N_{agg} was found with the help of accurate theoretical expressions. (The contact angle of a thin liquid film is sensitive to the acting surface forces, and the oscillatory force is sensitive to the micelle volume fraction ϕ.) The error in the contact-angle measurement is maximum ±0.05°, which yields an error of ±1 in N_{agg}. This error is somewhat below the range of N_{agg} changes. At 133 and 150 mM Brij 35, the values of N_{agg} are determined from the fits of the CP-AFM data in the present paper to the theoretical dependence in section 3. The used single adjustable parameter, ϕ, is related to N_{agg} by eq 17. If we substitute in the computer program a mean value, e.g., $N_{agg} = 69$, instead of 71 and 72 determined from the best fits, the agreement between theory and experiment visibly worsens. Hence, the weak tendency of N_{agg} to increase with the rise of the Brij 35 concentration seems to be a real one, but it is just slightly above the experimental error. Note also that the N_{agg} values in Table 1 and in ref 12 and are determined by two different methods (CP-AFM vs contact-angle measurements), but they are in good agreement.

A general feature of the experimental curves in Figures 1−4 is that they consist of alternating *equilibrium* and *nonequilibrium* portions. In contrast, the theoretical curve is completely equilibrium and it could coincide with the respective experimental curve

(86) Balescu, R. *Equilibrium and Nonequilibrium Statistical Mechanics*; Wiley: New York, 1975.
(87) Anderson, V. J.; Lekkerkerker, H. N. W. *Nature* **2002**, *416*, 811–815.

Table 1. Micelle Diameter, d, Volume Fraction, ϕ, Aggregation Number, N_{agg}, and the Dimensionless Oscillatory Amplitude, w_0, Wavelength, λ, and Decay Length, q^{-1}, vs the Brij 35 Concentration, C_s[a]

C_s (mM)	d (nm)	ϕ	N_{agg}	w_0	$\lambda = 2\pi/\omega$	q^{-1}
80	8.8	0.257	67	1.365	1.070	0.594
100	8.8	0.315	69	1.700	1.026	0.742
133	8.8	0.401	71	2.305	0.967	1.059
150	8.8	0.445	72	2.664	0.938	1.337
200	12[b]	0.483[b]		3.001	0.913	1.759

[a] λ and q^{-1} are scaled with the particle diameter, d, whereas w_0 is scaled with kT/d^2. [b] Effective values for elongated micelles − see section 4.2.

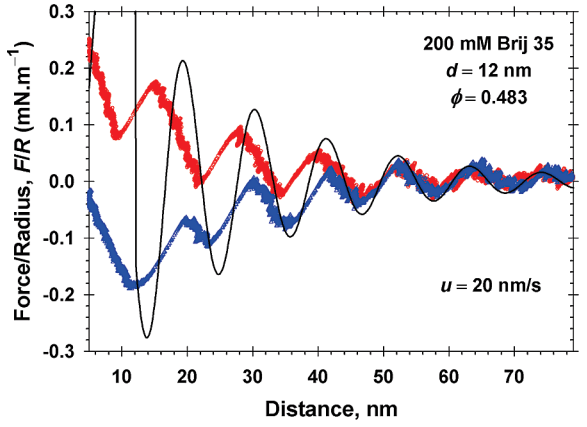

Figure 5. Force F vs distance H for a 200 mM Brij 35 solution that contains elongated micelles of effective hydrodynamic diameter $d = 12$ nm. The points are CP−AFM data; the upper and lower experimental curves are obtained, respectively, at approach and retraction. The solid line is a fit drawn by eqs 3−16 using the micelle volume fraction ϕ as a single adjustable parameter.

only at its equilibrium portions. One of the benefits from the comparison of theory with experiment is that it enables one to identify the equilibrium and nonequilibrium portions of the experimental curves. It is clearly seen that the nonequilibrium portions represent jumps from a given branch of the equilibrium theoretical curve to the next one. Because these jumps happen relatively quickly, the experimental curve contains a lower number of points in its nonequilibrium parts, which look thinner in the graphs. This is another way to distinguish between the equilibrium (thicker) and nonequilibrium (thinner) portions of a given experimental curve.

The experimental curves show a strong repulsion at short distances at about 8−10 nm (Figures 2−4). This distance is close to the micellar diameter. The simplest explanation is that a last layer of micelles remains between the two surfaces and cannot be pressed out. At 80 mM Brij35 (Figure 1), the repulsion is less steep and the distances can be reduced down to 5 nm. This could mean that the micelles in the last layer can be deformed due to the high load and could explain why the hysteresis between approach and retraction is so large. The micelles have more or less the same aggregation number irrespective of their concentration. But at low concentrations the micelles can be easier deformed due to more surrounding space, while it is more difficult to deform them in a laterally dense layer of micelles.

4.2. Results for Brij 35: Elongated Micelles. The experimental results by Tomšič et al.[88] indicate that at concentration 200 mM Brij 35 the micelles are elongated rather than spherical. The dynamic light scattering (DLS)[88] gives effective (or hydrodynamic) micelle diameter $d = 12$ nm. The latter value corresponds to hypothetic spherical micelles that have the same diffusivity as the mean diffusivity of the elongated micelles.

The AFM data for concentration 200 mM Brij 35 are presented in Figure 5. As it could be expected, the experimental curves have oscillatory behavior. We tried to fit the equilibrium portions of the curve in Figure 5 with the theoretical model for hard spheres, eqs 3−16. We found that this is possible only at greater distances, $H > 50$ nm, where the data can be fitted using the diameter of the effective spherical micelles, $d = 12$ nm, and adjusting the effective micelle volume fraction ϕ. The obtained value is $\phi = 0.483$ for the best fit.

At shorter distances ($H < 50$ nm), it was impossible to fit the data with eqs 3−16. The period of the theoretical curve for hard spheres is independent of the film thickness; i.e., ω in eq 9 is independent of H. In Figure 5, the theoretical curve, obtained by fitting the data for $H > 50$ nm, is extrapolated at shorter distances and is compared with the experimental curves at $H < 50$ nm. This comparison indicates that the measured curves have a varying period, which increases with the decrease of H. In other words, at shorter distances we are dealing with nonharmonic oscillations. In particular, the slope of the stable branches of the experimental curves is considerably smaller that that of the theoretical curve for hard spheres. Such behavior can be explained with the additional rotational degree of freedom of the elongated micelles. The spatial confinement forces the micelles to orient their long axes parallel to the film surfaces. In such a case, the film thickness can decrease not only by expulsion of micellar layers from the film but also by a gradual reorientation of the elongated micelles. The latter circumstance could explain the observed "softening" of the oscillatory interaction between the two solid surfaces at shorter distances.

4.3. Results for Tween 20. In ref 12, the stepwise thinning (stratification) of free foam films from micellar Tween 20 solutions was investigated. At 200 mM Tween 20, four steps were registered[12] by the Mysels-Jones porous-plate method,[17] and eight steps, by the Scheludko−Exerowa capillary cell.[89] Here, the CP-AFM was applied to Tween 20 micellar solutions to directly detect the oscillatory force that engenders the aforementioned stepwise transitions. For Tween 20, the CP-AFM does not detect such well-pronounced oscillatory behavior as with Brij 35 (Figures 1−5 above). The data in Figure 6 have been obtained at two relatively low force measuring velocities: $u = 5$ and 10 nm/s. As seen in the figure, only one well-pronounced jump has been registered. Among 120 runs, only a few experimental curves were detected that exhibit signs of oscillatory behavior. Below a speed of 5 nm/s, the noise was too large to detect oscillations and above 10 nm/s also no oscillations were detected. In Figure 6, the experimental curves at approach and retraction (150 mM Tween 20) were compared to the theoretical curve calculated without using any adjustable parameters. The values $d = 7.2$ nm and $N_{agg} = 70$ ($\phi = 0.250$), determined in ref 12, have been used.

Qualitatively similar experimental curves have been obtained for adsorbed micelles.[82] The data in Figure 6 indicate that the experimental force is close to that predicted by the theory for mobile (nonadsorbed) micelles, but the possible presence of adsorbed micelles cannot be ruled out.

The difference between the AFM experimental curves obtained for Brij 35 and Tween 20 micellar solutions indicates that the micelles of Tween 20 are more *labile* (as compared to those of Brij 35) and are demolished by the shear stresses engendered by the hydrodynamic flows in the liquid film. Indeed, the lack of

(88) Tomšič, M.; Bešter-Rogač, M.; Jamnik, A.; Kunz, W.; Touraud, D.; Bergmann, A.; Glatter, O. *J. Phys. Chem. B* **2004**, *108*, 7021–7032.

(89) Scheludko, A.; Exerowa, D. *Kolloid-Z* **1959**, *165*, 148–151.

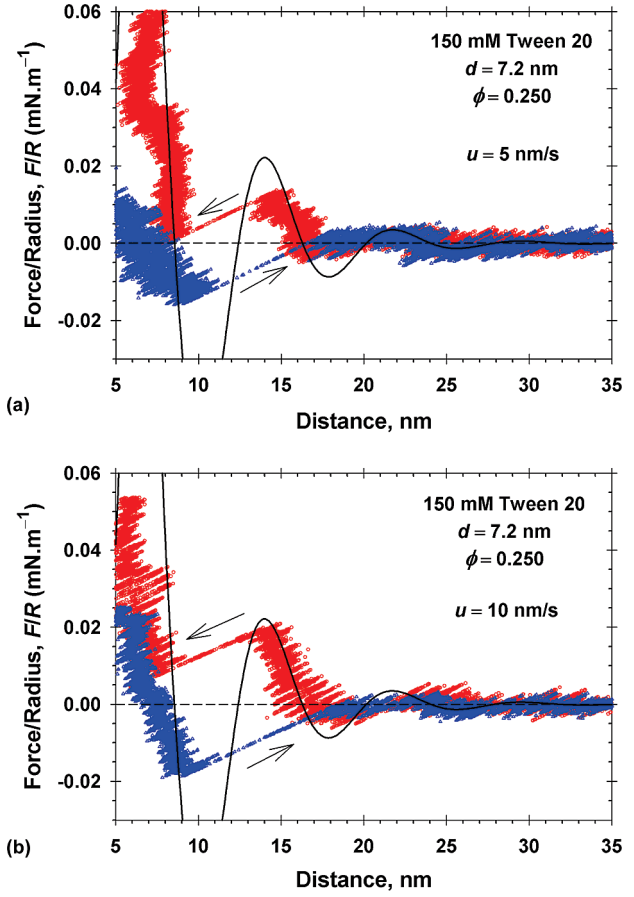

Figure 6. Force F vs distance H for 150 mM Tween 20 solutions. The points are CP−AFM data for two runs: (a) and (b); the arrows show the direction of measuring motion. The solid line is the theoretical curve drawn by means of eqs 3−16 without using adjustable parameters.

oscillatory behavior means absence of structural units (i.e., micelles) in the film. The scanning frequencies used in the experiments varied from 0.05 to 0.4 Hz; i.e., the film thinning/thickening continues from 2.5 to 20 s. In contrast, in ref 12 the spontaneous thinning of free films in the capillary cell takes more than 4000 s. In this respect, the capillary-cell method[89] and the thin film pressure balance method[17,90] are much milder (as compared to the CP-AFM), because the slow hydrodynamic flows in the spontaneously thinning films are accompanied by weak shear stresses that do not cause decomposition of the Tween 20 micelles in view of the well pronounced stepwise shape of the experimental curves obtained by these methods.[12]

The conclusion that the micelles of Tween 20 are more labile as compared to those of Brij 35 (see above) is supported by the measured relaxation time of the slow micellar process, τ_2, which characterizes the relaxation of the concentration of micelles in the course of their decomposition to monomers upon a sudden dilution.[91,92] The stopped-flow dilution technique yields $\tau_2 = 6$ s for Tween 20, and $\tau_2 = 80$ s for Brij 35; see Table 1 in ref 93. In other words, if the surfactant concentration is suddenly decreased, the perturbations in the concentrations of Tween 20 and Brij 35 micelles exponentially decay with characteristic times 6 and 80 s, respectively. Hence, the micelles of Tween 20 are destroyed much faster, which is in agreement with our conclusion that they are more labile.

4.4. Differences between the Cases of Nonionic Micelles and Charged Particles. Both types of systems lead to oscillatory force curves. In the case of nonionic micellar solutions, which behave as a hard-sphere fluid, the oscillatory period depends relatively weakly on the volume fraction ϕ; see the values of λ in Table 1. In contrast, for charged particles the period depends much stronger on particle concentration. For example, in the case of charged silica particles of diameter 9−25 nm, the oscillation period shows a strong dependence of the particle volume fraction[30,94] and scales as $\phi^{-1/3}$. The period corresponds to the distance of the particles in bulk solutions, obtained from the position of the structure peak of scattering spectra. The experimental results are in good agreement with Monte Carlo simulations using a grand canonical potential and lead to the conclusion that the interactions between the nanoparticles can be described with the simple potential of screened Coulomb interaction. In zero-order approximation, one could assume[6] that the effective diameter of a charged particle includes the Debye thickness, κ^{-1}, of the counterion atmosphere, $d_{\text{eff}} = 2(R + \kappa^{-1})$, where R is the particle hydrodynamic radius. The increase of ϕ leads to increase of the ionic strength due to counterions dissociated form the charged particles; then κ^{-1} and d_{eff} decrease. Note, however, that the above simple expression for d_{eff} does not provide quantitative description of the data from experiments with stratifying films, with charged particles and numerical simulations. Additional investigations are necessary in this field.

Another difference between micelles and solid particles is in the scan rate during the measurements. While the optimum scan rate in the case of nonionic micelles is quite low (100 nm/s and lower), one has to use a high scan rate (several 100s of nm/s) to observe oscillations with solid particles.[59]

5. Summary and Conclusions

In the present study, the oscillatory forces in micellar solutions of the nonionic surfactants Brij 35 and Tween 20 were measured using the CP-AFM. These forces cause stepwise thinning (stratification) of foam and emulsion films, and they can stabilize the liquid films and disperse systems under certain conditions.[9−12] Experimental force curves have been obtained at both approach and retraction of the colloidal probe. They are compared with the respective theoretical curves that correspond to a hard-sphere model.[54] For surfactant concentrations where the micellar volume fraction was already known (Figures 1, 2, and 6), the theoretical curves are drawn without using any adjustable parameters. In other cases (Figures 3−5) the micelle volume fraction, ϕ, had been determined from the fit of the data as a single adjustable parameter. From the obtained values of the micelle volume fraction, the micellar aggregation number, N_{agg}, was determined; it was about 70 for Brij 35 and slightly increase with the rise of surfactant concentration (Table 1).

With increasing surfactant concentration, both the amplitude and decay length of the force oscillation increases which indicates increasing ordering of the micelles (Table 1). In addition, the attraction between the surfaces at short distances (the depth of the first minimum) increases with increasing surfactant concentration, which leads to a strong hysteresis between the regimes of approach and retraction. The attraction can be such strong that

(90) von Klitzing, R. *Adv. Colloid Interface Sci.* **2005**, *114*, 253–266.
(91) Aniansson, E. A. G.; Wall, S. N. *J. Phys. Chem.* **1974**, *78*, 1024–1030.
(92) Danov, K. D.; Kralchevsky, P. A.; Denkov, N. D.; Ananthapadmanabhan, K. P.; Lips, A. *Adv. Colloid Interface Sci.* **2006**, *119*, 1–16.
(93) Patist, A.; Kanicky, J. R.; Shukla, P. K.; Shah, D. O. *J. Colloid Interface Sci.* **2002**, *245*, 1−15.
(94) Klapp, S. H. L.; Qu, D.; von Klitzing, R. *J. Phys. Chem. B* **2007**, *111*, 1296–1303.

several oscillations detected during approach can be jumped over, when the cantilever detaches from contact.

The comparison of theory and experiment gives the complete picture of the investigated phenomenon, provides new information and contributes to a deeper understanding of the observed processes. The experiment gives only parts of the stable branches of the oscillatory force-vs-distance dependence, whereas the theoretical model allows us to reconstruct the full curve, which allows a detailed analysis of the micellar ordering. In particular, by superimposing a given experimental curve on the theoretical one, the point of probe/substrate contact (i.e., the zero on the distance axis) could be accurately determined. At $H \approx d$, a strong repulsion is detected which leads to the conclusion that the system cannot overcome the first (the highest) maximum and one layer of micelles remains between the surfaces and cannot be pressed out. At low concentration of Brij35 (80 mM), the surfaces can be approached down to at least 5 nm and the hysteresis is even greater than for higher concentrations (Figure 1). This could mean that at low concentrations the micelles are deformed under the heavy load at short distances.

In the case of elongated micelles, which are present in the Brij 35 solutions at higher concentrations,[88] the experimental data do not show a harmonic oscillation anymore (Figure 5). This can be attributed to the circumstance that the film thickness can decrease not only by expulsion of micellar layers from the film but also by a gradual reorientation of the elongated micelles parallel to the film surfaces.

With Tween 20, the experimental curves do not have such well pronounced oscillatory behavior as with Brij 35. This fact indicates that the micelles of Tween 20 are much more labile than those of Brij 35 and are demolished by the shear stresses engendered by the hydrodynamic flows during the thinning or thickening of the liquid film. In contrast, in the case of Brij 35, the micelles are sufficiently stable, and the experimentally obtained oscillatory curves agree well with the theoretical predictions for a hard-sphere fluid. This behavior correlates with the characteristic times of the slow micellar relaxation process for the two surfactants (section 4.3).

Acknowledgment. This study is a result of cooperation in the framework of the EU COST Action D43. A partial support from Project DO-02-167/2008 of the National Science Fund of Bulgaria is gratefully acknowledged. Y.Z. and R.v.K. thank the German Research Council (DFG) for financial support (CRG 448, B10).